

Dynamics of ballistic photocurrents driven by Coulomb scattering

Liang Z. Tan,¹ Xavier Andrade,² Sangeeta Rajpurohit,¹ Alfredo A. Correa,² and Tadashi Ogitsu²

¹*Molecular Foundry, Lawrence Berkeley National Laboratory*

²*Quantum Simulations Group, Lawrence Livermore National Laboratory, Livermore CA 94551, USA*

First principles real-time time dependent density functional theory (rt-TDDFT) calculations reveal the existence of ballistic photocurrents generated by Coulomb scattering, a form of photocurrent that has not previously been considered as a mechanism for the bulk photovoltaic effect. With monolayer GeS as an example, it is predicted that ballistic currents can exceed shift currents under experimentally accessible conditions. Moreover, these simulations reveal recombination pathways that work to modify shift current magnitudes beyond perturbation theory predictions.

The bulk photovoltaic effect (BPVE) is the generation of a direct current in an extended material under photoexcitation, independent of interfacial effects [1]. Following early work to understand photocurrents in ferroelectrics [2], this field [3] has recently experienced a revival, driven by advances in first-principles computation [4], and the recasting of its response theory to the modern language of wavefunction geometry [5–8]. The BPVE is a light-harvesting mechanism operating outside the constraints [9] of conventional photovoltaics, such as the Shockley-Queisser limit [10]. It can also be used as a powerful mode of light-matter control or detection via its sensitive dependence to light polarization and frequency.

The shift current has been identified as one of the major contributions to the BPVE in some materials [4]. It is current generated directly by photoexcited transitions between valence and conduction bands. Much research on the BPVE operates within the assumption that the BPVE is dominated by the shift current [11]. Within perturbation theory, the shift current of a perfect crystal of non-interacting electrons appears to have no dependence on carrier scattering effects. However, recent work has revealed that shift current is strongly modified by scattering once these stringent conditions are removed [12, 13], with consequences for real materials with a number of intrinsic and extrinsic scattering sources.

The importance of scattering is further highlighted when considering BPVE arising from relaxation and recombination dynamics [14, 15]. Of these effects, ballistic photocurrents stand out for being driven entirely by scattering [16–20]. Here, carrier imbalance is established by scattering processes that break inversion symmetry. Theories for ballistic current driven by electron-phonon interactions [21, 22] as well as some experiments [23] suggest that ballistic photocurrents may account for a significant portion of the total BPVE in some materials. On the other hand, previous theories for ballistic current driven by electron-hole scattering have not predicted strong ballistic currents, although only under weak-field assumptions inherent to perturbation theory [24].

In this paper, we re-examine BPVE from the perspective of real-time TDDFT [25], free from the assumptions of weak-field or weak-scattering. We find that ballistic photocurrents driven by Coulomb scattering are a major component of BPVE, even exceeding the shift cur-

rent under some experimentally accessible conditions. By Coulomb scattering, we refer to the finite lifetime acquired by electrons and holes as they interact with the electronic charge density. As this form of scattering is intrinsic to any material, our results are likely to generalize to a wide range of materials. Furthermore, we treat both current components on the same footing and show how they can be differentiated by their intensity- and frequency-dependence. Previous real-time simulations [22, 26–29] of photocurrent and time-resolved experiments [30] have been useful for understanding transient photocurrent response, due to their nonperturbative and non-equilibrium nature. However, the explicit identification of the Coulomb ballistic current as a major BPVE mechanism has not previously been made, as it requires a careful partition of separate current components.

In rt-TDDFT, the current operator is represented by its matrix elements

$$\xi_{mm'}^{(0/1)}(\vec{k}, t) = \int d^3r \psi_{m\vec{k}}^{(0/1)*}(\vec{r}) \left(\vec{\nabla} - i\vec{A}(t) + [V_{\text{NL}}, \vec{r}] \right) \psi_{m'\vec{k}}^{(0/1)}(\vec{r}) \quad (1)$$

for instantaneous ($\psi^{(1)}$) orbitals and ground state ($\psi^{(0)}$) Kohn-Sham orbitals respectively, where $\vec{A}(t)$ is the uniform vector potential and V_{NL} is the nonlocal part of the Hamiltonian introduced by the pseudopotentials. The total current of an N -electron system is then given by

$$\vec{J}(t) = \text{Im} \sum_{\vec{k}} \text{Tr} \left[\rho^{(1)} \xi^{(1)}(\vec{k}, t) \right] \quad (2)$$

where $\rho^{(1)}$ is the density matrix in the basis of $\psi^{(1)}$, with nonzero elements $\rho_{nn} = f_n = 1$ for $n \leq N$ and 0 elsewhere.

To decompose the total photocurrent into shift and ballistic components, we expand it in the basis of ground state Kohn-Sham bands [28], introducing the density matrix in the ground state basis $\rho^{(0)} = U(t)\rho^{(1)}U^\dagger(t)$, with overlap matrix elements $U_{mn}(t) = \langle \psi_{m\vec{k}}^{(0)} | \psi_{n\vec{k}}^{(1)}(t) \rangle$, and writing the current as

$$\vec{J}(t) = \text{Im} \sum_{\vec{k}; m, m'=1}^M \left[\rho^{(0)} \right]_{m'm} \xi_{mm'}^{(0)}(\vec{k}, t) \quad (3)$$

We separate the band diagonal contributions ($m = m'$) to Eq. 3

$$\bar{J}^b(t) = \text{Im} \sum_{\vec{k}} \text{Tr} \left[\rho^{(0)} \odot \xi^{(0)}(\vec{k}, t) \right] \quad (4)$$

where \odot denotes the element-wise product of matrices, and the band off-diagonal contributions to the current, $\bar{J}^s(t) = \bar{J}(t) - \bar{J}^b(t)$, with “s” and “b” denoting the shift and ballistic components. This partition of the current is basis-dependent; the ground state basis $\psi^{(0)}$ is chosen to make contact with shift/ballistic current concepts which are defined as perturbations from the ground state. This partition is not dependent on basis rotations of the instantaneous occupied or unoccupied subspace separately, i.e., $\psi_{n'k}^{(1)} = W_{n'n} \psi_{nk}^{(1)}$ with $[\rho^{(1)}, W] = 0$, as required by gauge-invariance of the physical system.

The ballistic photocurrent is identified with the band diagonal contributions to the photocurrent, as Eq. 4 can be written as a product of projected occupation numbers with band velocities, $\bar{J}^b(t) = \sum_{nk} \tilde{f}_{nk}(t) v_{nk}$, with $\tilde{f}_{nk}(t) = [U(t) \rho U^\dagger(t)]_{m'm}$, in accordance with the historical perturbative definition of the ballistic current [14, 31]. Shift current has been identified as being driven by coherences (band off-diagonal density matrix elements) using perturbation theory arguments [1, 11].

To test the predictions of perturbation theory, we perform ab-initio rt-TDDFT simulations of photocurrents in monolayer GeS. This is a two-dimensional polar material which has previously been identified as a candidate with strong in-plane shift currents [27, 32]. With the out-of-plane normal as the x -direction, it has a mirror plane in the y -direction and a strong ground state polarization in the z -direction. Therefore, its photocurrent is expected to be the strongest in the z -direction.

In the following, we consider the longitudinal (z) photocurrent under monochromatic light linearly polarized in the z -direction, using resonant excitation frequencies from 2.0 eV to 3.2 eV, above the DFT band gap of 1.64 eV. The continuous wave excitation is smoothly turned on at $t = 0$ fs by convolving with a hyperbolic tangent function with a width of $\eta = 0.1$ fs, in order to avoid discontinuities in the dynamics. The resulting dynamics is insensitive to η in the range 0.1-1.0 fs. rt-TDDFT is performed with the PBE exchange-correlation functional, using norm conserving pseudopotentials, in the planewave basis at a kinetic energy cutoff of 50 Ha, and with a time step of 0.5 attosecond, as implemented in the INQ code [33, 34]. Using a supercell geometry, the ion positions are fixed and the lattice constants are kept constant at $(a_x, a_y, a_z) = (15.0, 3.603, 4.523)$ Å throughout the trajectory. A k -point grid of $2 \times 8 \times 32$ is sufficient for computing photocurrent under these conditions.

Due to computational limitations, the partition into j^b and j^s requires a finite cutoff on the number of ground state Kohn-Sham orbitals. For this, we used a total of $M = 40$, comprising 20 occupied bands and 20 unoccupied bands. j^b and j^s computed separately by taking the

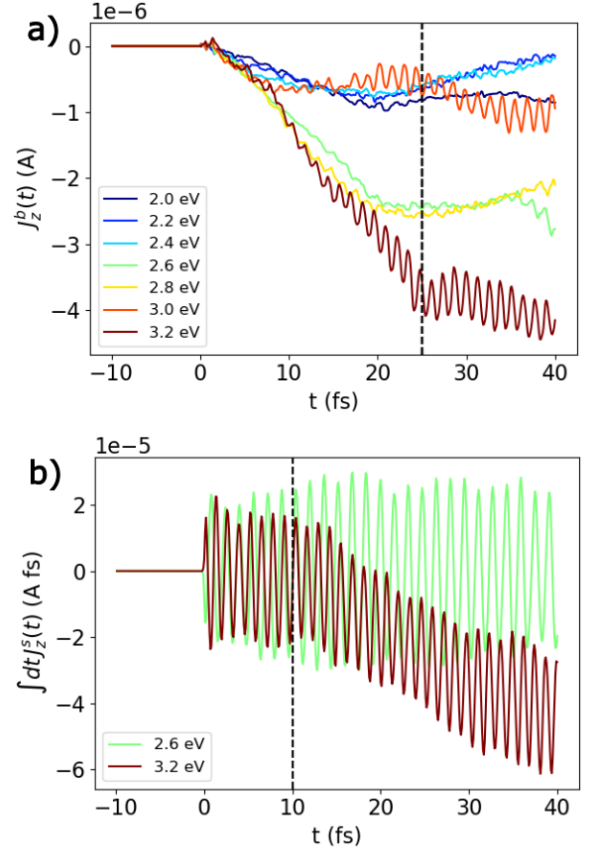


FIG. 1. a) Band diagonal photocurrent time-dependence of monolayer GeS under monochromatic continuous wave excitation with varying frequency and electric field strength 3.17 V/nm, turned on at $t = 0$. Vertical line denotes onset of current saturation (τ) under 3.2 eV excitation. b) Band off-diagonal contribution to the photocurrent under the same excitation conditions, displayed as a time-integral to illustrate changes in the direct current (dc) component. A linear rise in the time-integrated current indicates a steady current state. Vertical line denotes crossover to a state with higher off-diagonal current (t_c).

diagonal and off-diagonal elements of Eq. 3 are insensitive to further increase of M , with their sum agreeing with the total current Eq. 2 computed without the band cutoff, indicating that electronic populations and coherences from higher lying bands are unimportant.

Over a trajectory of 40 fs, we find that diagonal current first increases linearly for all excitation energies. The duration of this initial rise and the behavior after depends on the excitation energy. Then, the current either saturates and remains steady or it starts decreasing (Fig. 1a). According to perturbation theory, ballistic current is expected to increase linearly with time at short times [35], with the steady state current given by $\tau dJ^b/dt$ for some relaxation time scale τ . In GeS, we estimate the relaxation times to be in the range 10 fs - 30 fs. We attribute this relaxation to electron-charge density (e-d) Coulomb

scattering because electron-phonon scattering is removed by fixing the ionic degrees of freedom in these simulations. The saturation of ballistic current is not related to bleaching of the conduction/valence bands as it is observed even when carrier occupations are far from unity at low intensities (Supplemental Material). Besides the steady ballistic current, we also observe oscillations in J^b which increase with intensity. These are a result of higher order processes which will not be discussed further as they do not contribute to net current.

The off-diagonal $j^s(t)$ contribution has a different time-dependence (Fig. 1b). Its leading contributions are oscillations at the driving frequency, corresponding to direct absorption. The zero-frequency (shift) current is typically much smaller, although nonzero and quantifiable by simulations. At certain frequencies, such as 3.2 eV, the system transitions from a state with low shift current at short times ($t < t_c$) to a state with larger, but steady shift current ($t > t_c$). This crossover time $t_c = 10$ fs is distinct from the ballistic current relaxation time.

To understand these phenomena, we examine contributions to J^b and J^s across k -points and bands. Partitioning the total current as $\vec{J}(t) \equiv \sum_{\vec{k}; m, m'=1}^M j_{m, m'}(\vec{k}, t)$, in Fig. 2 we plot the symmetrized ballistic current contribution $j_m^b(k, t) = (j_{m, m}(k, t) + j_{m, m}(-k, t))/2$ and the symmetrized shift current contribution per band $j_m^s(k, t) = \sum_{n \neq m} [j_{n, m}(k, t) + j_{m, n}(k, t) + j_{n, m}(-k, t) + j_{m, n}(-k, t)]/4$, alongside instantaneous carrier occupations. The antisymmetrized currents are not considered as their total does not contribute any current.

By comparing carrier occupations at $t = 10$ fs and $t = 30$ fs, we see that carriers are initially excited via resonant transitions (Fig. 2b, and Supplemental Material), before relaxing via e-d scattering to isolated locations in the Brillouin zone (Fig. 2e). These accumulation points tend to be located near van Hove singularities because of limited phase space for scattering there, but do not necessarily need to be at the valence band maximum or the conduction band minimum, such as near the Γ point of the second valence band in Fig. 2e. Accumulations points are the most apparent for the excitation frequency of 3.2 eV compared to other frequencies (Supplemental Material), likely as a result of specific scattering pathways that are activated at this frequency. When other relaxation processes are included, such as electron-phonon interactions, and at longer times, it is expected that there will be a greater tendency for relaxation to energy band extrema. Nevertheless, these results show that electron-density scattering drives transient carrier dynamics to band locations which affect ballistic and shift currents.

We find that ballistic current is mostly concentrated where carrier occupations are high, and where there is sufficient carrier velocity, such as along the Γ -Z and R -Y lines. This is consistent with the usual perturbative interpretation of ballistic current. In this picture, it is the antisymmetrized carrier occupations $f^{asym} = f(k) - f(-k)$ that carry photocurrent, due to the time-reversal symmetry of band velocities $v_{n, k} = -v_{n, -k}$. We find that

ballistic current is larger at locations of carrier excitation than at locations of carrier accumulation from relaxation. Despite the vicinity of the accumulation point at Γ having large carrier densities, it does not contribute much to ballistic current. This is because the antisymmetrized carrier occupations are much lower there than at the excitation surface (Supplemental Material). Even though the initial antisymmetry in carrier occupations at the excitation surface are induced by scattering, it is likely that the multiple scattering events required to bring those carriers to accumulation points diminishes antisymmetry.

Similar to the diagonal currents, the off-diagonal currents are mostly located where there are resonant transitions. There, the contributions to shift current can be separated into counteracting excitation and recombination terms, with the total shift current at that k -point being proportional to the difference of conduction and valence band occupation numbers [15, 36]. At the excitation frequency of 3.2 eV, the second valence band at Γ is special in being both a resonant k -point as well as an accumulation point. We infer that the shift current at the second valence band at Γ is made up of direct excitation to the conduction bands as well as recombination from carriers scattered into Γ but originally excited elsewhere. The crossover time t_c is then explained by the transition from excitation shift current at short times to recombination shift current at longer times.

This picture is further supported by the intensity dependence of the measured currents. The rate of increase of ballistic currents before saturation ($t < \tau$) is linear with intensity E^2 (Fig. 3a), agreeing with perturbation theory [35]. The shift current measured at short times ($t < 5$ fs) scales with $\sqrt{E^2}$, while the shift current measured over the entire trajectory contains both $\sqrt{E^2}$ and E^2 components (Fig. 3bc). This agrees with predictions that shift currents scale as $\sqrt{E^2}$ in the Rabi (high-field) regime, and as E^2 in the low-field regime [13]. The Rabi regime is characterized by the inequality $E \langle \psi_m^{(0)} | r | \psi_n^{(0)} \rangle \tau \gg 1$ [13]. Based on the different time-dependence of these two intensity components we assign them different shift current mechanisms. The excitation shift current, which is the only shift current contributions active at short times, is in the Rabi regime for this material under these excitation conditions. The recombination shift current arising from carrier scattering from elsewhere in the Brillouin zone, which is only active at later times, is in the low-field regime. Indeed, the E^2 intensity dependence is the strongest for the excitation frequency 3.2 eV, which has the most apparent recombination shift current identified from the band structure plots (Fig 2, Supplemental Material). These results indicate that ballistic and different components of the shift currents may exist in different non-perturbative regimes even under the same excitation conditions.

The energy dependence at early-times (Fig. 3a) and at steady state (Fig. 1a) of the ballistic current can be drastically different, as the relaxation time τ is highly energy dependent, suggesting that constant relaxation time ap-

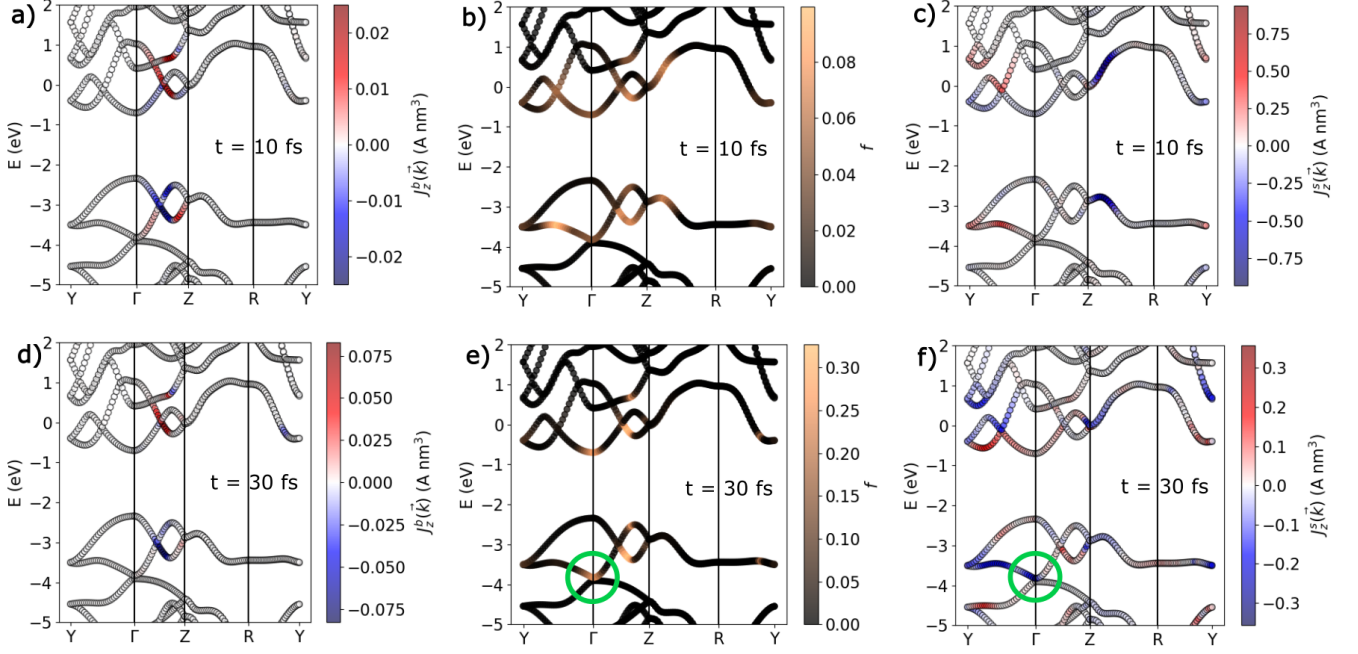


FIG. 2. Band structure of monolayer GeS with instantaneous band diagonal photocurrent, carrier occupation number, and band off-diagonal photocurrent superimposed, for $t = 10$ fs after the start of continuous wave photoexcitation (a-c), and $t = 30$ fs after the start of continuous wave photoexcitation (d-f). Green circles in (e) and (f) highlight accumulation point of carrier density, and associated contribution to band off-diagonal photocurrents, respectively. Monochromatic excitation is at frequency 3.2 eV and electric field strength 3.17 V/nm.

proximations are insufficient. The energy dependence of the high-field early-time shift current show multiple sign-changes (Fig. 3b), consistent with previous time-domain simulations which are likely to be in the high-field Rabi regime [27], and contrasting with perturbation theories applicable to the low-field regime [32].

Recombination shift currents [15, 36] are active even in the absence of scattering. Considering only the $\sqrt{E^2}$ scaling components in Fig. 3bc, their magnitudes are generally reduced over the entire length of the trajectory compared to at short times only. This is because of the rise in band occupation numbers at resonant k -points at later times activates recombination currents there.

Over the course of the simulations, the maximum magnitude of ballistic currents rises to 4.2×10^{-6} A (Fig. 1), while the shift current transiently reaches a similar magnitude at 4.6×10^{-6} A (Fig. 3). These results show that ballistic currents arising from e-d scattering accounts for a large portion of the total BPVE, being comparable to shift current at short times and becoming much larger at longer times when shift current is diminished due to its recombination component. The optical responsivity of the ballistic current, $\sigma = J/(b(E/\epsilon)^2)$, is estimated by taking the ballistic current at the time of saturation (τ), with $b = a_x a_y$ being the cross-sectional area. In this definition we use the screened electric field E/ϵ , for a fair comparison with perturbative calculations where the effect of screening is not typically included in the response

tensor. In rt-TDDFT, screening is naturally included in the transient response of the charge density. At the excitation frequency of 3.2 eV, and with the computed in-plane dielectric constant of $\epsilon = 5.5$, we estimate the ballistic current optical responsivity to be 2.3×10^{-5} A/V², to be compared with the shift current optical responsivity of $\sim 1 \times 10^{-4}$ A/V² obtained from perturbation theory [32]. As our rt-TDDFT simulations show, the actual shift current present in the material will be reduced from this perturbative prediction because of the crossover to $\sqrt{E^2}$ scaling shift current and the presence of recombination shift currents.

Switching to a real-space picture, we partition the photocurrent into contributions from separate real-space points (Eq. 1). This is done separately for the diagonal and off-diagonal currents. We find that ballistic photocurrent flow consists of vortex-like structures near atom cores which do not contribute to total current, as well as global flows present in the interstitial regions which do contribute to the total current (Fig. 4). This delocalized interstitial current density is a reflection of the asymmetric carrier occupations responsible for the ballistic photocurrent. For the off-diagonal photocurrent, the real-space contributions are comparatively more localized near the atom cores, arising from band-to-band transitions between atomic-like orbitals (Supplemental Material). A similar distinction between laminar and disordered flow lines has been observed in simulations of

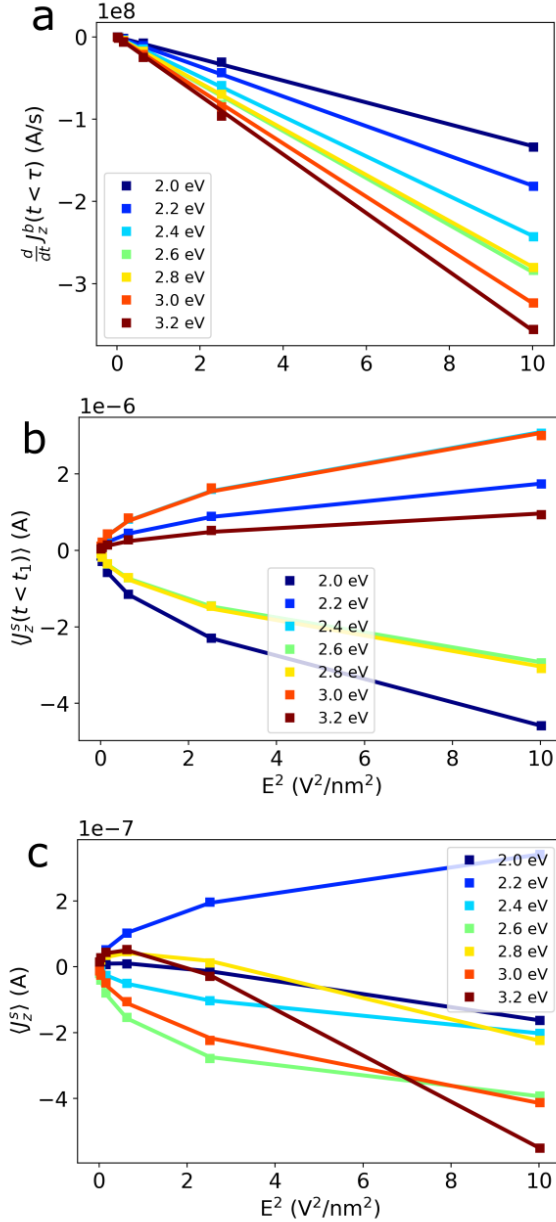


FIG. 3. a) Rate of change of band diagonal photocurrent at early times showing linear scaling with light intensity, for varying excitation energies. Colored lines are linear fits of data points. b) Zero-frequency component of band off-diagonal photocurrent at early times showing square-root scaling with light intensity, for varying excitation energies. Colored lines are fits of data points to a square-root function. c) Zero-frequency component of band off-diagonal photocurrent calculated over the entire trajectory as a function of light intensity, for varying excitation energies. Colored lines are fits of data points to a function with linear and square root terms.

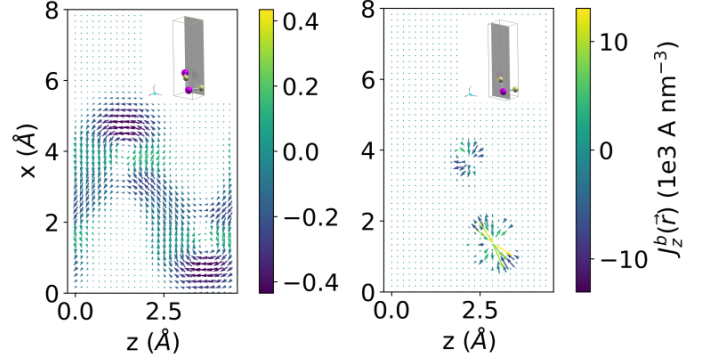


FIG. 4. Real-space current densities of band diagonal photocurrent plotted in the mirror planes $y = 0$ (left) and $y = 2.7 \text{ \AA}$ (right). The mirror plane $y = 2.7 \text{ \AA}$ intersects a pair of Ge and S atoms, shown in the inset. Direction of arrows show the projection of current density to the $x - z$ plane, while the color depicts the z -component of the current density. Current density was calculated at excitation energy 2.8 eV and electric field strength 1.59 V/nm, at $t = 30$ fs after the start of excitation.

nonlinear conductivity in metals [37].

In summary, we have observed ballistic currents generated by Coulomb scattering in rt-TDDFT simulations. These currents are comparable in magnitude to shift currents. We find that recombination currents strongly affect the total shift current, but appear to be less important for ballistic currents. These observations suggest that a multitude of mechanisms contribute to the BPVE, with consequences for understanding many experiments beyond the narrow interpretation of the excitation shift current. The ballistic current optical responsivity from Coulomb scattering measured here is similar to that from electron-phonon scattering [24], which is expected considering that both forms of scattering have similar overall scattering rates [38], and suggesting that other forms of scattering, such as from defects or interfaces, could potentially contribute strongly to ballistic photocurrents as well. While we have shown that the Coulomb ballistic current is already present at the mean-field approximation, the effects of electron-electron correlation also warrants further study. The range of time scales revealed by these simulations, associated with the rise and changes of the various photocurrents, and transient accumulation points of carriers, suggests that ultrafast experiments will greatly aid the understanding of these phenomena.

ACKNOWLEDGMENTS

Theory and simulation were supported by the Computational Materials Sciences Program funded by the US Department of Energy, Office of Science, Basic Energy Sciences, Materials Sciences and Engineering Division. Additional data analysis was supported by a user project at the Molecular Foundry was supported by the Office

of Science, Office of Basic Energy Sciences, of the U.S. Department of Energy under Contract No. DE-AC02-05CH11231. This research used resources of the National Energy Research Scientific Computing Center, a DOE Office of Science User Facility supported by the Office

of Science of the U.S. Department of Energy under Contract No. DE-AC02-05CH11231. AAC, XA and TA work was performed under the auspices of the US Department of Energy by Lawrence Livermore National Laboratory under contract DE-AC52-07NA27344.

-
- [1] Z. Dai and A. M. Rappe, Recent progress in the theory of bulk photovoltaic effect, *Chemical Physics Reviews* **4**, 011303 (2023).
 - [2] R. von Baltz and W. Kraut, Theory of the bulk photovoltaic effect in pure crystals, *Physical Review B* **23**, 5590 (1981).
 - [3] V. I. Belinicher and B. I. Sturman, The photogalvanic effect in media lacking a center of symmetry, *Sov. Phys. Usp.* **23**, 199 (1980).
 - [4] S. M. Young and A. M. Rappe, First Principles Calculation of the Shift Current Photovoltaic Effect in Ferroelectrics, *Physical Review Letters* **109**, 116601 (2012).
 - [5] T. Morimoto and N. Nagaosa, Topological nature of nonlinear optical effects in solids, *Science Advances* **2**, e1501524 (2016).
 - [6] T. Morimoto, S. Kitamura, and N. Nagaosa, Geometric Aspects of Nonlinear and Nonequilibrium Phenomena, *Journal of the Physical Society of Japan* **92**, 072001 (2023), publisher: The Physical Society of Japan.
 - [7] J. Ahn, G.-Y. Guo, N. Nagaosa, and A. Vishwanath, Riemannian geometry of resonant optical responses, *Nature Physics* **18**, 290 (2022), number: 3 Publisher: Nature Publishing Group.
 - [8] A. Alexandradinata, A topological principle for photovoltaics: Shift current in intrinsically polar insulators (2022), arXiv:2203.11225v2.
 - [9] L. Z. Tan and A. M. Rappe, Upper limit on shift current generation in extended systems, *Physical Review B* **100**, 085102 (2019).
 - [10] W. Shockley and H. J. Queisser, Detailed Balance Limit of Efficiency of p-n Junction Solar Cells, *Journal of Applied Physics* **32**, 510 (1961).
 - [11] L. Z. Tan, F. Zheng, S. M. Young, F. Wang, S. Liu, and A. M. Rappe, Shift current bulk photovoltaic effect in polar materials—hybrid and oxide perovskites and beyond, *npj Computational Materials* **2**, 16026 (2016).
 - [12] T. Barik and J. D. Sau, Nonequilibrium nature of nonlinear optical response: Application to the bulk photovoltaic effect, *Phys. Rev. B* **101**, 045201 (2020), publisher: American Physical Society.
 - [13] O. Matsyshyn, F. Piazza, R. Moessner, and I. Sodemann, Rabi Regime of Current Rectification in Solids, *Phys. Rev. Lett.* **127**, 126604 (2021), publisher: American Physical Society.
 - [14] B. Sturman, Ballistic and shift currents in the bulk photovoltaic effect theory, *Phys. Usp.* 10.3367/UFNe.2019.06.038578 (2019), arXiv:1911.11940.
 - [15] P. Zhu and A. Alexandradinata, Anomalous shift and optical vorticity in the steady photovoltaic current (2023), arXiv:2308.08596v3.
 - [16] P. Král and J. E. Sipe, Quantum kinetic theory of two-beam current injection in bulk semiconductors, *Phys. Rev. B* **61**, 5381 (2000).
 - [17] V. V. Men'shenin, Phonon mechanism of the antiferromagnetic photogalvanic effect, *Phys. Solid State* **45**, 2131 (2003).
 - [18] E. Deyo, L. E. Golub, E. L. Ivchenko, and B. Spivak, Semiclassical theory of the photogalvanic effect in non-centrosymmetric systems, arXiv:0904.1917 [cond-mat] (2009), arXiv: 0904.1917.
 - [19] P. T. Mahon, R. A. Muniz, and J. E. Sipe, Quantum interference control of localized carrier distributions in the Brillouin zone, *Phys. Rev. B* **100**, 075203 (2019), publisher: American Physical Society.
 - [20] Y. Okamura, T. Morimoto, N. Ogawa, Y. Kaneko, G.-Y. Guo, M. Nakamura, M. Kawasaki, N. Nagaosa, Y. Tokura, and Y. Takahashi, Photovoltaic effect by soft phonon excitation, *Proceedings of the National Academy of Sciences* **119**, e2122313119 (2022), publisher: Proceedings of the National Academy of Sciences.
 - [21] Z. Dai, A. M. Schankler, L. Gao, L. Z. Tan, and A. M. Rappe, Phonon-Assisted Ballistic Current from First-Principles Calculations, *Phys. Rev. Lett.* **126**, 177403 (2021), publisher: American Physical Society.
 - [22] S. Rajpurohit, T. Ogitsu, and L. Z. Tan, Ballistic photocurrent driven by optical phonon modes in a polaronic ferroelectric, *Phys. Rev. B* **108**, 104305 (2023), publisher: American Physical Society.
 - [23] A. M. Burger, R. Agarwal, A. Aprelev, E. Schrubba, A. Gutierrez-Perez, V. M. Fridkin, and J. E. Spanier, Direct observation of shift and ballistic photovoltaic currents, *Science Advances* **5**, eaau5588 (2019).
 - [24] Z. Dai and A. M. Rappe, First-principles calculation of ballistic current from electron-hole interaction, *Phys. Rev. B* **104**, 235203 (2021), publisher: American Physical Society.
 - [25] E. Runge and E. K. U. Gross, Density-functional theory for time-dependent systems, *Physical Review Letters* **52**, 997–1000 (1984).
 - [26] Y. Miyamoto, Visualizing Electron–Hole Separation in Photo-excited Polar Crystals, *Appl. Phys. Express* **3**, 047202 (2010), publisher: IOP Publishing.
 - [27] Y.-H. Chan, D. Y. Qiu, F. H. da Jornada, and S. G. Louie, Giant exciton-enhanced shift currents and direct current conduction with subbandgap photo excitations produced by many-electron interactions, *Proceedings of the National Academy of Sciences* **118**, e1906938118 (2021), publisher: Proceedings of the National Academy of Sciences.
 - [28] F. He, X. Ren, S. Meng, and L. He, Ultrafast shift current dynamics in WS₂ monolayer (2022), arXiv:2207.03772 [cond-mat].
 - [29] S. Rajpurohit, C. Das Pemmaraju, T. Ogitsu, and L. Z. Tan, Nonperturbative study of bulk photovoltaic effect enhanced by an optically induced phase transition, *Phys. Rev. B* **105**, 094307 (2022), publisher: American Physical Society.

- [30] S. Priyadarshi, K. Pierz, and M. Bieler, All-Optically Induced Ultrafast Photocurrents: Beyond the Instantaneous Coherent Response, *Phys. Rev. Lett.* **109**, 216601 (2012).
- [31] V. I. Belinicher and B. I. Sturman, The relation between shift and ballistic currents in the theory of photogalvanic effect, *Ferroelectrics* **83**, 29 (1988).
- [32] T. Rangel, B. M. Fregoso, B. S. Mendoza, T. Morimoto, J. E. Moore, and J. B. Neaton, Large Bulk Photovoltaic Effect and Spontaneous Polarization of Single-Layer Monochalcogenides, *Phys. Rev. Lett.* **119**, 067402 (2017).
- [33] X. Andrade, C. D. Pemmaraju, A. Kartsev, J. Xiao, A. Lindenberg, S. Rajpurohit, L. Z. Tan, T. Ogitsu, and A. A. Correa, Inq, a Modern GPU-Accelerated Computational Framework for (Time-Dependent) Density Functional Theory, *J. Chem. Theory Comput.* **17**, 7447 (2021), publisher: American Chemical Society.
- [34] X. Andrade, C. D. Pemmaraju, A. Kartsev, J. Xiao, A. Lindenberg, S. Rajpurohit, L. Z. Tan, T. Ogitsu, and A. A. Correa, Inq, a library for tddft numerical simulations on hpc and gpus (2024), <https://gitlab.com/npneq/inq>.
- [35] J. E. Sipe and A. I. Shkrebtii, Second-order optical response in semiconductors, *Physical Review B* **61**, 5337 (2000).
- [36] V. I. Belinicher, E. L. Ivchenko, and B. I. Sturman, Kinetic theory of the displacement photovoltaic effect in piezoelectric, *JETP* **56**, 359 (1982).
- [37] X. Andrade, S. Hamel, and A. A. Correa, Negative differential conductivity in liquid aluminum from real-time quantum simulations, *The European Physical Journal B* **91**, 229 (2018).
- [38] M. Bernardi, D. Vigil-Fowler, J. Lischner, J. B. Neaton, and S. G. Louie, \textit{Ab~Initio} Study of Hot Carriers in the First Picosecond after Sunlight Absorption in Silicon, *Physical Review Letters* **112**, 257402 (2014).

Supplementary Information for
Dynamics of ballistic photocurrents driven by Coulomb scattering

Liang Z. Tan,¹ Xavier Andrade,² Sangeeta

Rajpurohit,¹ Alfredo A. Correa,² and Tadashi Ogitsu²

¹*Molecular Foundry, Lawrence Berkeley National Laboratory*

²*Lawrence Livermore National Laboratory, Livermore, USA*

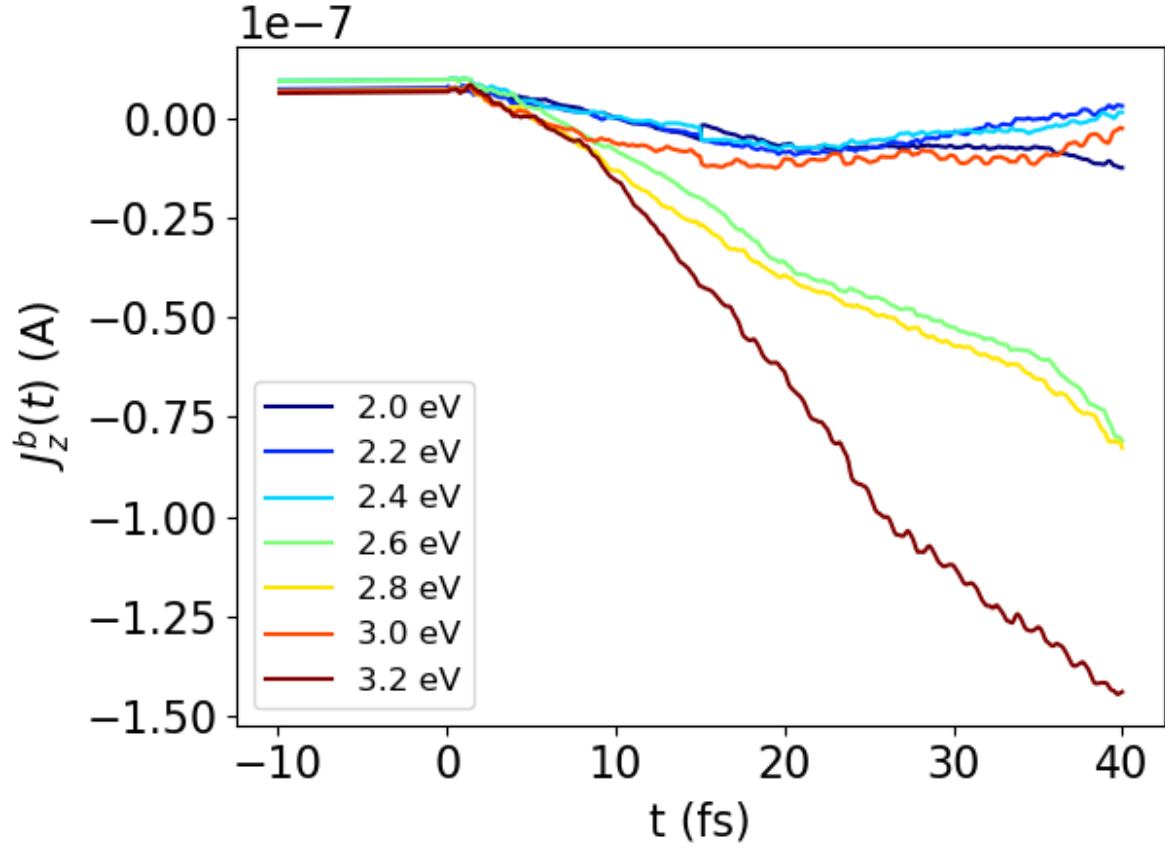


FIG. 1. Band diagonal photocurrent time-dependence of monolayer GeS under monochromatic continuous wave excitation with varying frequency and electric field strength 0.399 V/nm, turned on at $t = 0$. Even at this reduced intensity, the band diagonal photocurrent still saturates within the simulation time for some excitation frequencies.

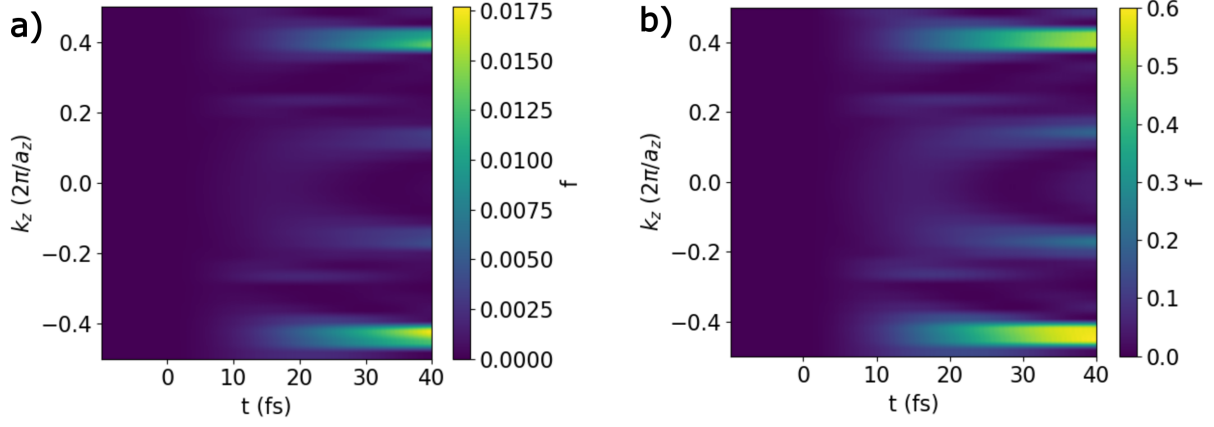


FIG. 2. Occupation of the lowest conduction band along the $k_x = 0, k_y = 0$ line, at frequency 3.0 eV, at electric field strengths 0.399 V/nm (a) and 3.17 V/nm (b).

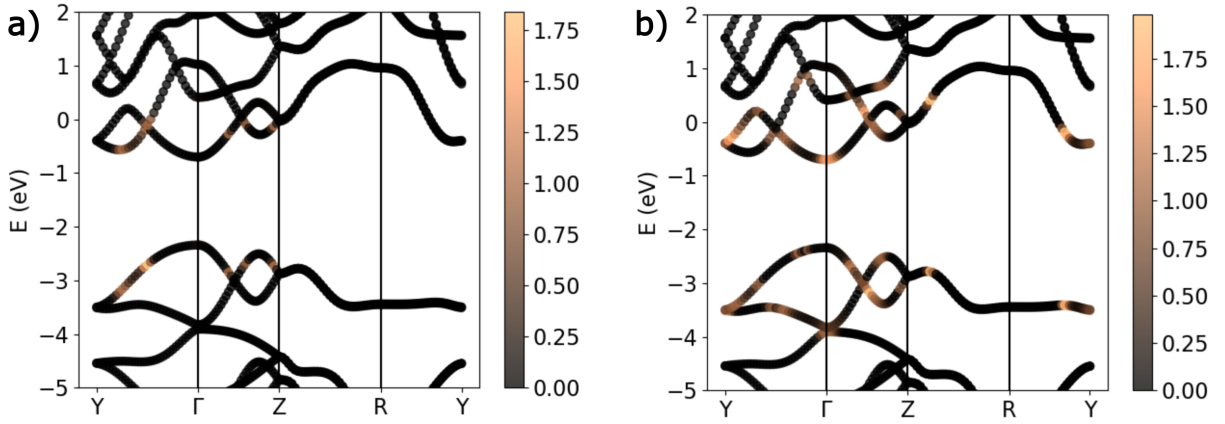


FIG. 3. Plot of resonant transitions at (a) 2.4 eV and (b) 3.2 eV. Colored points denote bands that participate in resonant transitions at these frequencies.

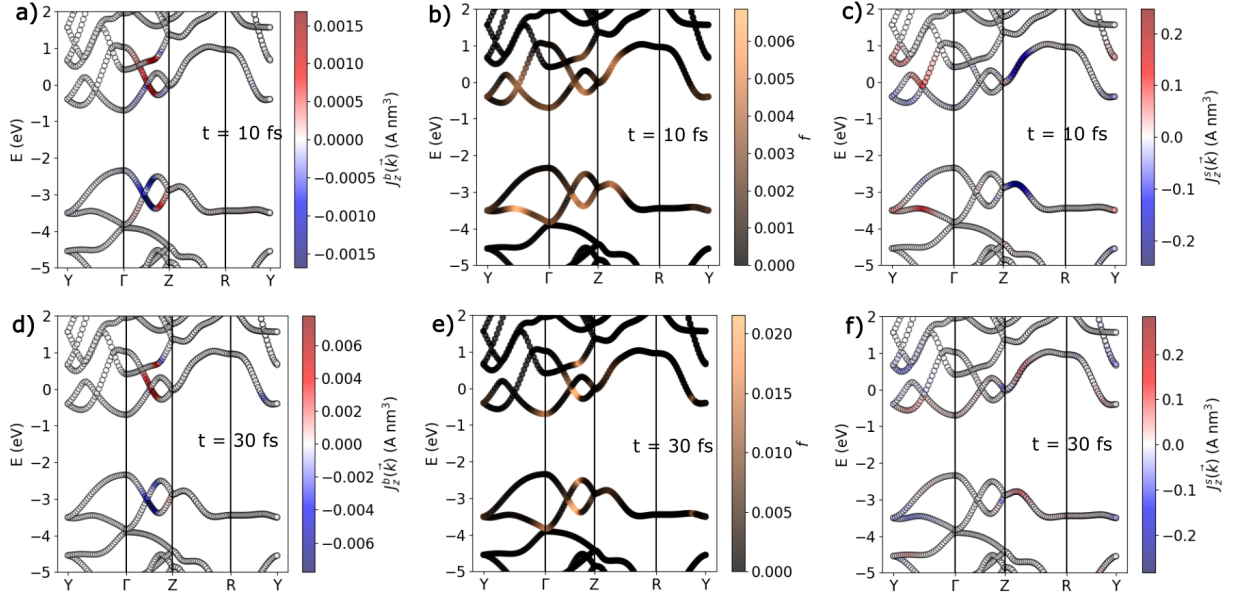


FIG. 4. Under monochromatic excitation at frequency 3.2 eV and electric field strength 0.795 V/nm, band structure of monolayer GeS with instantaneous band diagonal photocurrent, carrier occupation number, and band off-diagonal photocurrent superimposed, for $t = 10$ fs after the start of continuous wave photoexcitation (a-c), and $t = 30$ fs after the start of continuous wave photoexcitation (d-f).

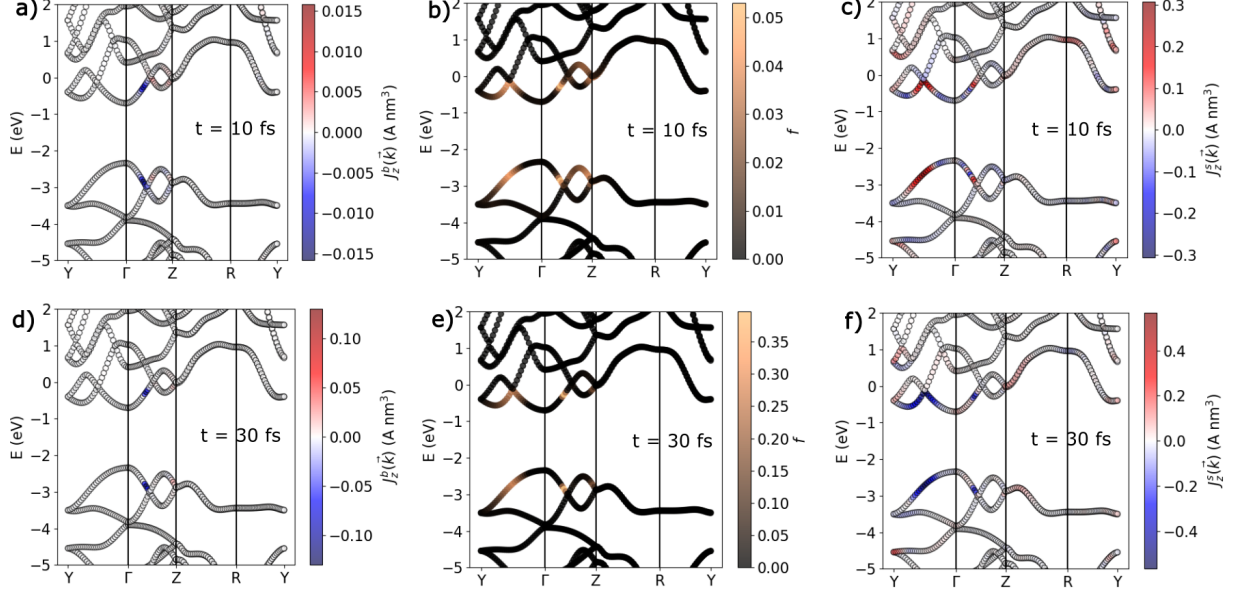


FIG. 5. Under monochromatic excitation at frequency 2.6 eV and electric field strength 3.17 V/nm, band structure of monolayer GeS with instantaneous band diagonal photocurrent, carrier occupation number, and band off-diagonal photocurrent superimposed, for $t = 10$ fs after the start of continuous wave photoexcitation (a-c), and $t = 30$ fs after the start of continuous wave photoexcitation (d-f).

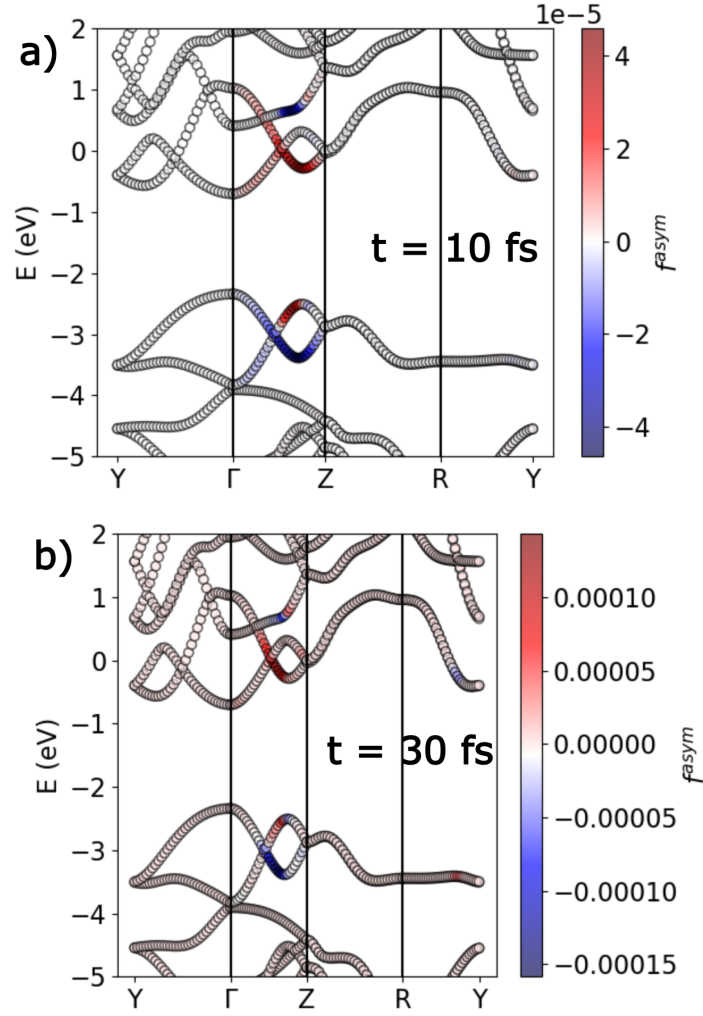


FIG. 6. Under monochromatic excitation at frequency 3.2 eV and electric field strength 3.17 V/nm, band structure of monolayer GeS with instantaneous asymmetrized carrier occupation number $f^{asym} = f(k) - f(-k)$, for $t = 10$ fs after the start of continuous wave photoexcitation (a), and $t = 30$ fs after the start of continuous wave photoexcitation (b).

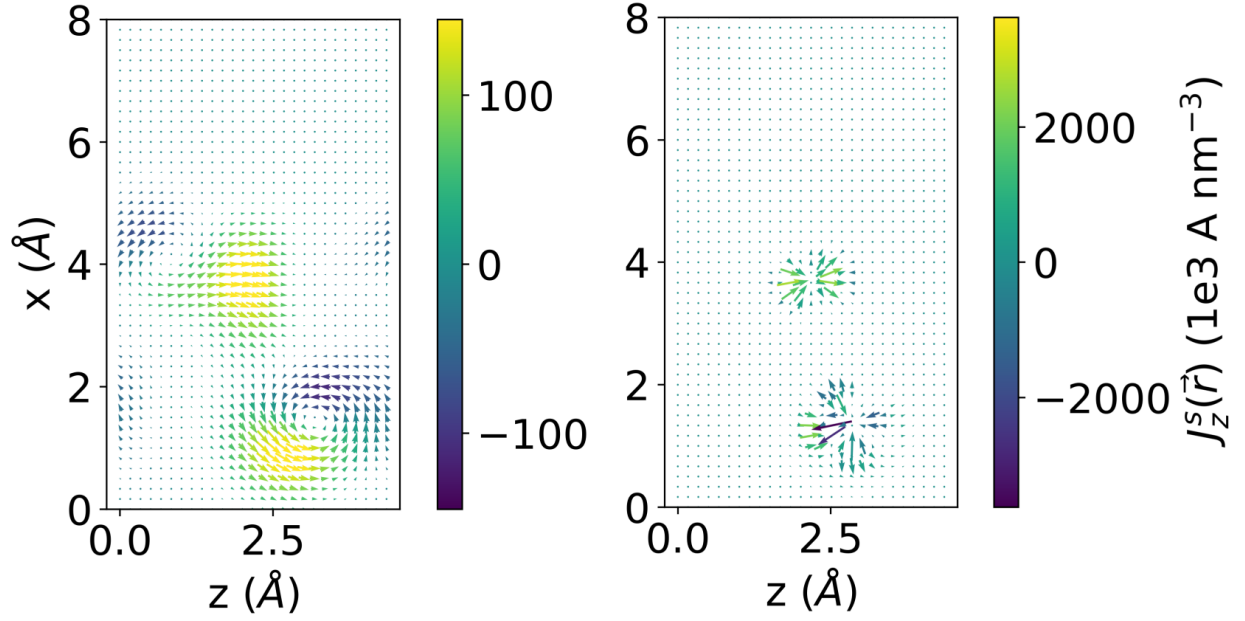


FIG. 7. Real-space current densities of band off-diagonal photocurrent plotted in the mirror planes $y = 0$ (left) and $y = 2.7\text{\AA}$ (right). The mirror planes are in the same location as in Fig. 4 of the main text. Direction of arrows show the projection of current density to the $x - z$ plane, while the color depicts the z -component of the current density. Current density was calculated at excitation energy 2.8 eV and electric field strength 1.59 V/nm, at $t = 30$ fs after the start of excitation.